Journal of Power Sources 219 (2012) 89–93

Contents lists available at SciVerse ScienceDirect

Journal of Power Sources

journal homepage: www.elsevier.com/locate/jpowsour

Simple synthesis of metallic Sn nanocrystals embedded in graphitic ordered mesoporous carbon walls as superior anode materials for lithium ion batteries

Yangang Wang [a,*], Bo Li [b], Chengli Zhang [b], Hong Tao [a], Shifei Kang [b], Sheng Jiang [b], Xi Li [b,**]

[a] School of Environment and Architecture, University of Shanghai for Science and Technology, 516# Jungong Road, Shanghai 200093, China
[b] Department of Environmental Science and Engineering, Fudan University, Shanghai 200433, China

HIGHLIGHTS

- A simple solid–liquid grinding/templating method is used for the synthesis of Sn–C nanocomposite.
- Sn nanocrystals with the sizes of 3–5 nm are embedded in graphitic ordered mesoporous carbon walls.
- The new Sn–C nanocomposite as an anode material exhibits excellent electrochemical performance.

GRAPHICAL ABSTRACT

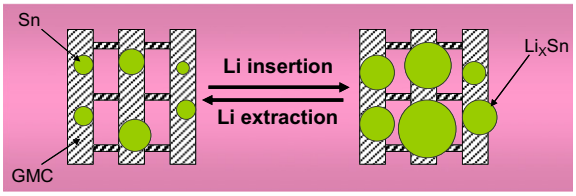

ARTICLE INFO

Article history:
Received 21 April 2012
Received in revised form
23 May 2012
Accepted 16 July 2012
Available online 24 July 2012

Keywords:
Tin–graphitic mesoporous carbon
Solid–liquid grinding/templating
Anode materials
Lithium ion batteries

ABSTRACT

New Sn–C nanocomposite with metallic tin nanocrystals embedded into graphitic mesoporous carbon walls has been synthesized via a simple one-step solid–liquid grinding/templating route. X-ray diffraction, nitrogen adsorption–desorption, transmission electron microscopy and thermogravimetric analysis techniques are used to characterize the samples. It is observed that high content of metallic tin nanocrystals with the sizes of 3–5 nm are well dispersed into the highly conductive graphitic carbon walls, and synthesized tin–graphitic mesoporous carbon (Sn–GMC) nanocomposite possesses ordered 2D hexagonal mesostructures with moderate surface area, large pore volume and hierarchical porosity. Due to its novel structures, the Sn–GMC nanocomposite exhibits high initial coulombic efficiency, excellent cyclability and rate performance when employed as an anode material in lithium ion batteries.

1. Introduction

Rechargeable lithium-ion batteries (LIBs), which are currently the main power sources for portable electronic devices, are now considered as promising power supplies for electric vehicles and hybrid electric vehicles [1–4]. The new generation LIBs, which are expected to have superior performance in terms of energy density, cycling life, and rate capability, may only be obtained by achieving breakthroughs in electrode materials [5–8]. As one of the most promising anode materials, metallic Sn has received enormous research interest as potential substitute for current graphite electrode (theoretical capacity 372 mAh g^{-1}) because of its higher theoretical reversible specific capacity ($Li_{4.4}Sn$, 992 mAh g^{-1}) [1,9]. However, the commercial use of metallic Sn to LIBs is generally hindered by the severe volume change (259%) during Li^+ insertion/extraction cycle, which causes the disintegration of the electrode and rapid capacity fading [9,10]. In order to overcome this shortcoming, several efforts including using nano-sized metallic Sn particles [11,12], binary Sn-alloys [13,14], and Sn-based carbon composites [15–20] have been invested. In these cases, Sn-based carbon composites especially the nanostructured metallic Sn encapsulated in the carbon matrices have attracted particular attention since carbon materials can buffer the volume changes of

* Corresponding author. Tel./fax: +86 21 55275979.
** Corresponding author.
E-mail addresses: ygwang8136@gmail.com (Y. Wang), xi_li@fudan.edu.cn (X. Li).

0378-7753/$ – see front matter © 2012 Elsevier B.V. All rights reserved.
http://dx.doi.org/10.1016/j.jpowsour.2012.07.047

Sn particles and provide good electrical contact [21–23]. However, the fabrication of Sn/C nanocomposite reported to date usually involves complicated procedure, and the formed carbon matrices mostly are amorphous bulk without controllable porous structure which prevents the rapid Li^+ insertion/extraction during the discharge/charge cycles [17].

Ordered mesoporous carbons, due to its unique structural and chemical properties, have been recently considered as powerful nanomaterials to functionalize other electrode materials for improving their electrical conductivity, mechanical and thermal properties in LIBs [24,25]. For example, Zhao et al. [26] reported that the deposition of SnO_2 in the channels of mesoporous carbon CMK-3 by using impregnation method showed a better cycle performance than nano-sized SnO_2. By using such time consuming method, several other anode materials such as metallic Sn, CoO, and NiO nanoparticles incorporated into the amorphous mesoporous carbon channels were also prepared by other groups [16,27,28], their reports have resulted in improvements of the electrochemical performance of the anodes to some extents. However, because of the limited space of mesoporous channels, it is not feasible to load high content of anode materials on mesoporous carbon since the huge volume changes of big active particles during the discharge/charge cycles easily destroy the mesostructure of carbon supports which leads to a poor cycling performance [26]. Recently, Chen et al. [22] fabricated ordered mesoporous Sn–C composite with Sn nanoparticles confined in carbon nanorods via a nanocasting approach, such material exhibited excellent cycling and rate performances when employed as anode material in lithium ion batteries. However, because of its high surface area (583 $m^2 g^{-1}$) and amorphous carbon framework, a large initial irreversible capacity loss accompanied with low coulombic efficiency is inevitable.

Herein, we present a simple process for the synthesis of new Sn–C nanocomposite anode material with metallic Sn nanocrystals embedded in graphitic ordered mesoporous carbon (GMC) walls. The synthesis was achieved using one-step solid–liquid grinding/templating method developed by our group [29], during which ordered mesoporous silica SBA-15 was used as a template, soybean oil and tin bichloride dihydrate were respectively used as the carbon source and tin precursor. It was showed that highly dispersed metallic Sn nanocrystals with the sizes of 3–5 nm were well embedded into the highly conductive graphitic carbon walls, and the synthesized nanocomposite possesses ordered 2D hexagonal mesostructures with moderate surface area, large pore volume and hierarchical porosity. Preliminary experiments in this study showed that this new Sn–GMC nanocomposite exhibited improvement of initial coulombic efficiency, excellent cyclability and rate performance when employed as an anode material in lithium ion batteries.

2. Experimental

2.1. Synthesis of Sn–GMC nanocomposite

Ordered mesoporous silica SBA-15 template with rodlike morphology was synthesized as the reported procedure except enlarging the amount by ten times [30]. New Sn–GMC nanocomposite was synthesized using one-step solid–liquid grinding templating method without the help of any organic solvent. In a typical synthesis, ordered mesoporous silica SBA-15 template (5.0 g), soybean oil (10.0 g), and tin bichloride dehydrate ($SnCl_2 \cdot 2H_2O$, 3.5 g) were ground together for 4 h on a ball mill machine to get a homogeneous mixture, then the mixture was transferred into a tube furnace to carbonize the precursors at the temperature of 900 °C under Ar flow for 5 h with a heating rate of 2 °C min^{-1}, the resultant composites were treated with 2 M NaOH aqueous solution to remove the silica template. Graphitic ordered mesoporous carbon was prepared by the same method but without adding any tin salt in the above experimental process.

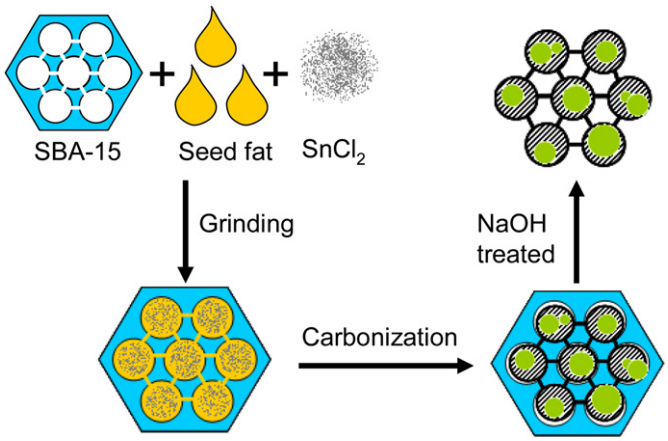

Fig. 1. Illustration of the synthesis of Sn–GMC nanocomposite by solid–liquid grinding/templating method.

2.2. Structural characterization

Small-angle X-ray diffraction (SXRD) patterns were collected in θ–2θ mode using Rigaku D/MAX-2550VB/PC diffractometer (Cu$K\alpha_1$ radiation, $\lambda = 1.5406$ Å), operated at 40 kV and 200 mA (scanning step: 0.02° per second). Wide-angle XRD patterns were collected in the same mode, but operated at 100 mA. Scanning electron microscopy (SEM) images were performed on a Philips XL-30 scanning electron microscope operating at an acceleration voltage of 25 kV. Transmission electron microscope (TEM) images were taken using a JEOL JEM-2010 electron microscope with an acceleration voltage of 200 kV. Nitrogen sorption isotherms were measured at −196 °C on a Micromeritics ASAP 2000 apparatus. Before measurements, the samples were degassed in vacuum at 200 °C for 6 h. The Brunauer–Emmett–Teller (BET) method was utilized to calculate the specific surface areas. The pore size distributions were derived from the desorption branches of the isotherms using the Barrett–Joyner–Halenda (BJH) method. The total pore volume (V_t) was estimated at a relative pressure of 0.98. Thermogravimetric analysis was carried out using a Mettler Toledo TGA–SDTA851 analyzer (Switzerland) from 25 to 800 °C in an air flow of 80 mL min^{-1} at a heating rate of 5 °C min^{-1}.

2.3. Electrochemical measurements

Electrochemical measurements were performed using home-made coin cells with lithium metal as the counter and reference electrodes at room temperature. The working electrodes were prepared by coating the slurry of the active materials (70 wt%), carbon black (20 wt%), and polyvinylidene fluoride (PVDF) (10 wt%) dissolved in n-methyl pyrrolidinone onto a Cu foil substrate. The coated electrodes were dried in a vacuum oven at 120 °C for 12 h and then pressed to enhance the contact between the active materials and the conductive carbons. The electrolyte was 1 M $LiPF_6$ in a mixture of ethylene carbonate and diethyl carbonate (1:1 by volume), and Celgard 2400 was used as the separator. Cell assembly was carried out in an argon-filled glove-box (with the concentrations of moisture and oxygen below 1 ppm). The electrochemical performance was tested at various C-rate regimes in the voltage range of 0.005–2.00 V on a NEWARE battery test system.

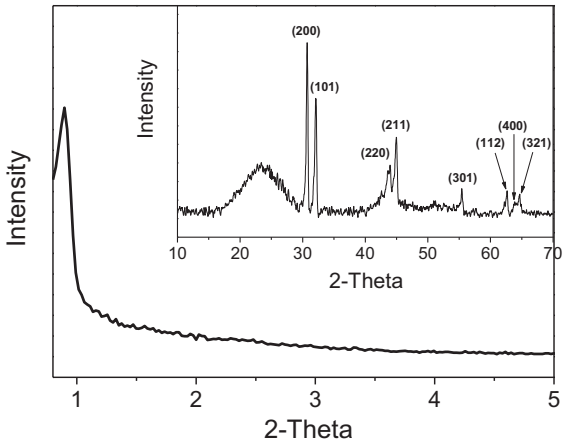

Fig. 2. Low-angle and wide-angle (inset) XRD patterns of the Sn–GMC nanocomposite.

3. Results and discussion

The synthesis process of the Sn–GMC nanocomposite by one-step solid–liquid grinding/templating method is very simple (illustrated in Fig. 1). Ordered mesoporous silica SBA-15, soybean oil and tin bichloride dihydrate with the weight ratio of 1:2:0.7 were ground together to get a homogeneous mixture. Heat treatment was carried out at 900 °C under Ar atmosphere with a gradual increase of temperature and Sn nanocrystals were reduced *in situ* and confined into the walls of mesoporous carbon accompanying the process of carbonaceous polymerization/graphitization, since the melting point of $SnCl_2 \cdot 2H_2O$ is only 37.7 °C much less than its boiling point (652 °C), it will infilter into the channels of mesoporous silica with soybean oil during the heat treatment. The silica template was removed with sodium hydroxide aqueous solution.

The formation of the Sn–GMC nanocomposite is firstly provided by X-ray diffraction (XRD) analysis as shown in Fig. 2. The low-angle XRD pattern in Fig. 2 shows that a sharp diffraction corresponding to (100) reflection of the 2D hexagonal ($p6mm$) symmetry can be observed, indicating that the synthesized Sn–GMC nanocomposite has retained regular mesostructures although the higher angle two diffractions indexed to (110) and (200) are too weak to be detected, as confirmed by the transmission electron microscope (TEM) images (see Fig. 3a). From the wide-angle XRD pattern (Fig. 2 inset), it can be seen that in addition to the two broad peaks at around 25 and 44° which can be respectively indexed to the (002) and (101) reflections for typical graphitic carbon, all diffraction peaks can be well indexed to pure β-Sn (JCPDS card no. 86-2265) and no evidence of tin oxide is detected. Here it should be mentioned that if the metallic Sn stays on the channels of mesoporous carbon, it will be gradually dissolved into the sodium hydroxide aqueous solution and change into corresponding stannonate under the experimental condition. TG result (Fig. S1) under air atmosphere exhibits that this Sn–GMC nanocomposite has a chemical composition of about 24.6 wt% metallic Sn and 75.4 wt% graphitic carbon, and the existence of high content of metallic Sn in the resultant nanocomposite reveals that metallic Sn is stable during NaOH treatment, which is due to the embedding of Sn nanocrystals into graphitic carbon matrix, and the latter protects the metal particles against environmental degradation.

The SEM images in Fig. S2 show that the rodlike morphology of the SBA-15 template is replicated in the Sn–GMC nanocomposite,

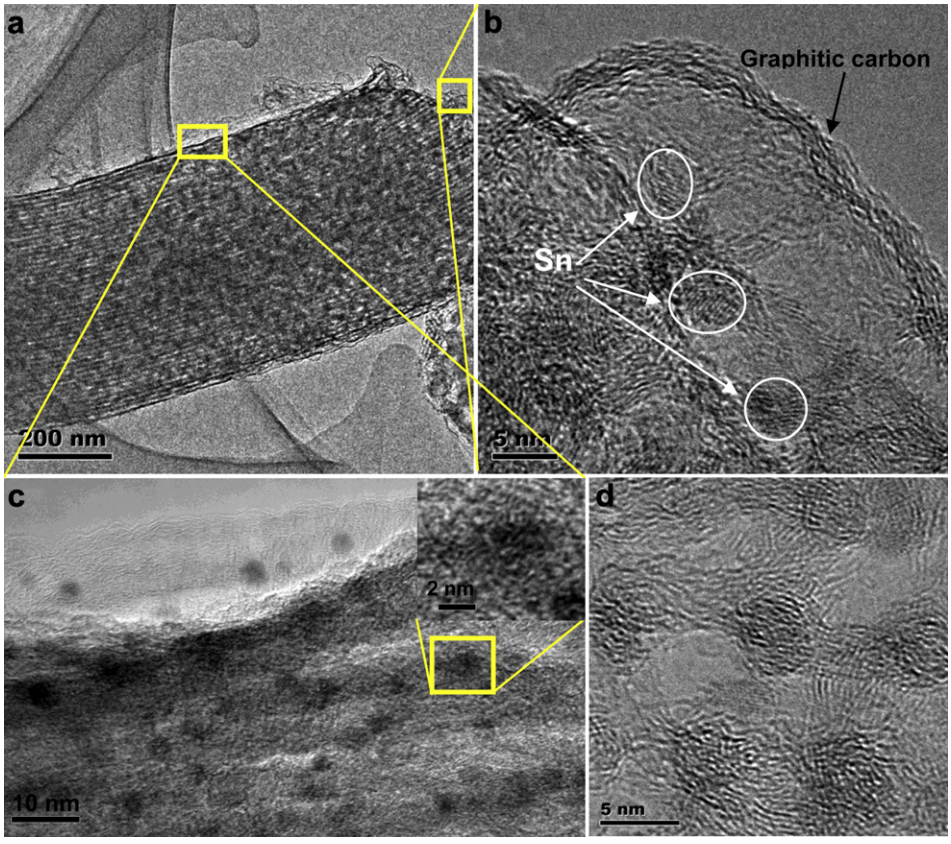

Fig. 3. Low- (a) and high-magnification (b, c) TEM images for the Sn–GMC nanocomposite. (d) HRTEM image long [100] direction.

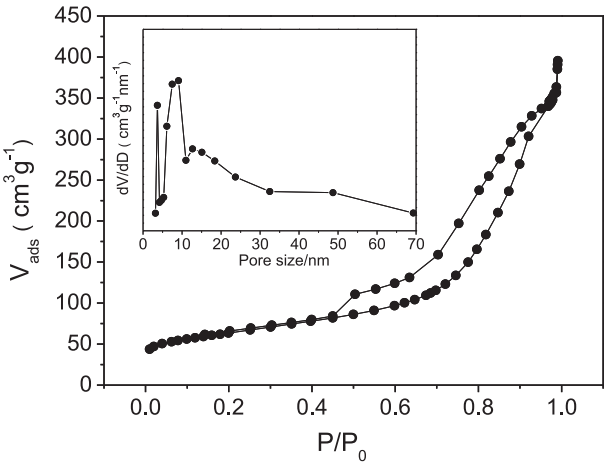

Fig. 4. N_2 adsorption–desorption isotherms of the Sn–GMC nanocomposite and the corresponding BJH pore size distribution curve (inset).

the average length of the rodlike Sn–GMC nanocomposite is about 1.2 μm which is similar to the hard template SBA-15 rods. The detailed structure was provided by TEM images. From the low-magnification image (Fig. 3a), it can be seen that besides the rodlike morphology, ordered 2D hexagonal mesostructure was clearly observed for the nanocomposite. However, there are no evident big particles that related to metallic Sn can be detected from low-magnification TEM images, indicating Sn with ultrafine nanocrystals is homodispersed in the graphitic mesoporous carbon. The further high-magnification TEM (HRTEM) images (Fig. 3b, c and the inset of Fig. 3c) show that metallic Sn nanocrystals are well embedded into the graphitic mesoporous carbon walls with the particle sizes of 3–5 nm, which is consistent with above deduction. HRTEM image along the [100] direction in Fig. 3d further confirms the embedded Sn nanocrystals and the opened mesopore channels. In addition, HRTEM images exhibit that the mesoporous carbon in nanocomposite has a relative high graphitic degree with the *d* spacing of the observed lattice planes of 0.345 nm and very close to the *d*(002) value (0.34 nm) of typical graphite, which is in agreement with our previous study [29]. This new architecture of Sn–C nanocomposite is important and useful in LIBs anode since graphitic carbon walls can function as efficient electron transport pathways and stable mechanical support for active metallic Sn, at the same time, it can also serve as an impediment against the deleterious reactions between active matter and solution species in discharging–charging processes due to the close contact of metallic Sn@graphitic carbon structure.

Fig. 4 gives the nitrogen adsorption–desorption isotherms and corresponding Barrett–Joyner–Halenda (BJH) pore size distribution curve for the Sn–GMC nanocomposite. A strong uptake of N_2 as a result of capillary condensation is observed in a wide relative pressure (P/P_0) range of 0.40–0.95, which is the characteristic of mesoporous materials. The pore size distribution obtained from an analysis of desorption branch of the isotherm is shown in the inset of Fig. 4. It can be seen that this nanocomposite has bimodal pore size distributions centered at about 3.8 and 8.1 nm which are respectively ascribed to the dissolution of the silica walls and the coalescence of no completely filled spaces of the template SBA-15. Such hierarchical mesostructure is especially valuable for lithium ion batteries system since ionic diffusion/transfer becomes easily. Additionally, the Sn–GMC nanocomposite has a moderate BET surface area ~223.9 $m^2\ g^{-1}$, and a large pore volume ~0.611 $m^3\ g^{-1}$, which may reduce the formation of solid electrolyte interface (SEI) films and provide a high coulombic efficiency during the initial Li^+ discharge/charge cycles.

In order to test the potential applicability of the prepared Sn–GMC nanocomposite in lithium ion batteries, the electrochemical performance of this material was tested in Sn–GMC/Li half cell (see details in experimental section). Fig. 5(a) displays typical

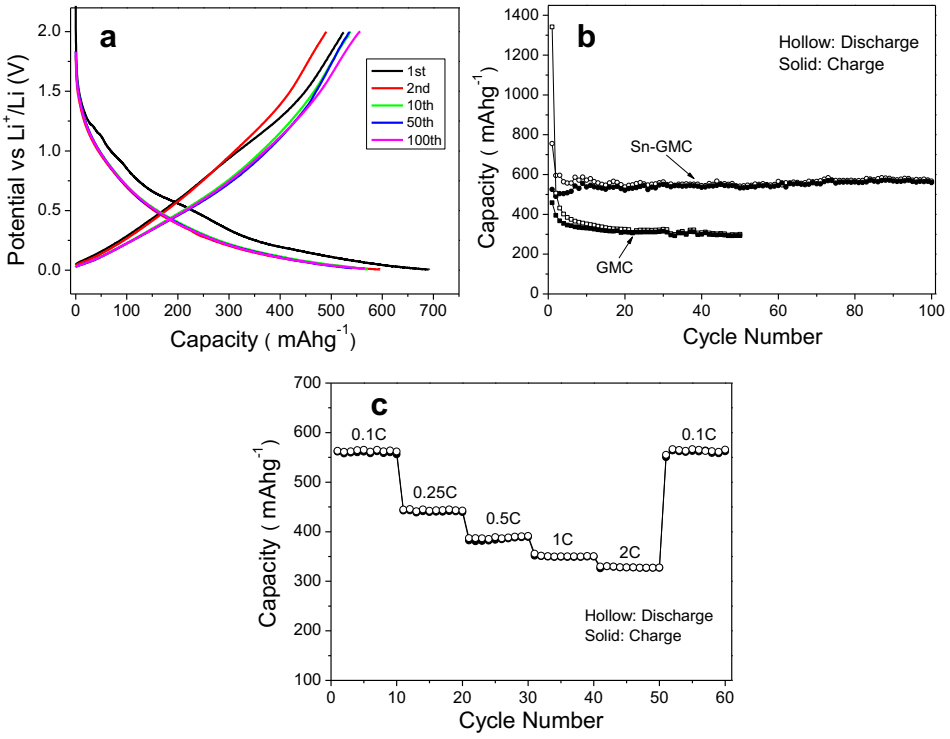

Fig. 5. (a) Typical discharge–charge voltage profiles of the Sn–GMC nanocomposite electrode at a current rate of 0.1 C; (b) Comparison of the cycle performances of the Sn–GMC nanocomposite and graphitic mesoporous carbon at a current rate of 0.1 C; (c) Rate capabilities of the Sn–GMC nanocomposite at various rates.

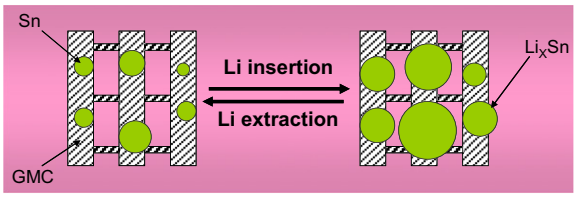

Fig. 6. Discharge (Li^+ insertion) and charge (Li^+ extraction) processes of the Sn–GMC electrode.

discharge–charge voltage profiles of the Sn–GMC nanocomposite electrode at a constant rate of 0.1 C. The Sn–GMC nanocomposite electrode shows first discharge and charge capacities of 691.4 mAh g^{-1} and 524.9 mAh g^{-1} in the voltage range of 0.005–2.0 V, corresponding to an initial columbic efficiency (ICE) of approximately 75.9%, which was notably higher than the previous studies on amorphous mesoporous carbon/metal oxide nanocomposites (generally ICE < 50%) [27,28]. The improvement of the ICE for Sn–GMC nanocomposite may result from the hierarchical mesostructures and the decreased formation of nonconducting solid electrolyte interface due to its relative low specific surface area.

The excellent cycle performance of the Sn–GMC nanocomposite is demonstrated in Fig. 5(b). For comparative purpose, a graphitic ordered mesoporous carbon (GMC) derived from soybean oil was prepared according to literature [29] and also examined under the same conditions. At the current rate of 0.1 C, the Sn–GMC nanocomposite exhibits high coulombic efficiency approaching 100% with a stable specific capacity of 560 mAh g^{-1} after 100 cycles, almost double the value for graphite. Whereas the capacity of GMC electrode gradually decreased to 290 mAh g^{-1} even after 50 cycles. Fig. 5(c) shows rate capacity for the Sn–GMC/Li half cell after 100 cycles. When the current rate is first increased from 0.1 to 0.25 C, a stable capacity of 445 mAh g^{-1} can be achieved. Afterward, the discharge–charge rates were continuously increased stepwise up to 2 C, under this high rate, the Sn–GMC nanocomposite can still deliver a stable capacity of about 330 mAh g^{-1} after 10 cycles. In other words, the discharge or charge process can be finished in about 30 min while still obtaining a relatively high capacity. Moreover, when the current rate is again returned to 0.1 C after more than 160 cycles, a stable high capacity of 560 mAh g^{-1} can be resumed, demonstrating that the Sn–GMC nanocomposite anode has an excellent rate performance.

Such pronounced electrochemical performance can be ascribed to the unique structure of the Sn–GMC nanocomposite with a variety of favorable properties, as shown in Fig. 6. First, monodispersed micro-rods with hierarchical mesostructures make facile the liquid electrolyte diffusion into the bulk of the electrode material and hence provides fast conductive ion transport channels for the conductive ions. Second, the graphitic carbon frameworks can well buffer against the local volume changes of metal active materials and sustain the hierarchical architecture due to the special metallic Sn@graphitic carbon structure. Finally, well-interconnected graphitic carbon matrix has a high electronic conductivity which ensures the good electrical contact of the electrode during cycling.

4. Conclusions

In conclusion, we have demonstrated for the first time that new Sn–C nanocomposite anode material with metallic Sn nanocrystals embedded in graphitic ordered mesoporous carbon walls was synthesized via a simple one-step solid–liquid grinding/templating route. XRD, nitrogen sorption, SEM, TEM and TG results all consistently reveal that the highly dispersed metallic Sn nanocrystals with the sizes of 3–5 nm are well embedded in the highly conductive graphitic ordered mesoporous carbon walls, and the obtained Sn–GMC nanocomposite possesses hierarchical mesostructures with moderate surface area and large pore volume which are beneficial for the electric and ionic diffusion/transfer and thereby result in the improvement of rate performance and cycling capability. Indeed, we have demonstrated that this new Sn–GMC nanocomposite used as advanced LIBs anode materials exhibited excellent electrochemical performances. In addition, our simple synthesis route can be easily enlarged and also extended to other graphitic mesoporous carbon–metal or metal oxides nanocomposite, these works are in process.

Acknowledgments

This work was supported by China Postdoctoral Science Foundation Funded Project (Grant No. 20100480534), China Postdoctoral Science Foundation Special Funded Project (Grant No. 201104236), Shanghai Pujiang Rencai Project (Grant No. 09PJ1401400), and the National Natural Science Foundation of China (Grant No. 21103024).

Appendix A. Supplementary material

Supplementary material associated with this article can be found, in the online version, at http://dx.doi.org/10.1016/j.jpowsour.2012.07.047.

References

[1] Y. Idota, T. Kubota, A. Matsufuji, Y. Maekawa, T. Miyasaka, Science 276 (1997) 1395–1397.
[2] J.M. Tarascon, M. Armand, Nature 414 (2001) 359–367.
[3] A.S. Arico, P. Bruce, B. Scrosati, J.M. Tarascon, W. Van Schalkwijk, Nat. Mater. 4 (2005) 366–377.
[4] M. Armand, J.M. Tarascon, Nature 451 (2008) 652–657.
[5] Y.G. Wang, H.Q. Li, Y.Y. Xia, Adv. Mater. 18 (2006) 2619–2623.
[6] P.G. Bruce, B. Scrosati, J.M. Tarascon, Angew. Chem. Int. Ed. 47 (2008) 2930–2946.
[7] C.K. Chan, H.L. Peng, G. Liu, K. McIlwrath, X.F. Zhang, R.A. Huggins, Y. Cui, Nat. Nanotechnol. 3 (2008) 31–35.
[8] Z.H. Wen, Q. Wang, Q. Zhang, J.H. Li, Adv. Funct. Mater. 17 (2007) 2772–2778.
[9] M. Winter, J.O. Besenhard, Electrochim. Acta 45 (1999) 31–50.
[10] Z. Peng, Z. Shi, M. Liu, Chem. Commun. 21 (2001) 2125–2126.
[11] J.O. Besenhard, J. Yang, M. Winter, J. Power Sources 68 (1997) 87–90.
[12] L. Bazin, S. Mitra, P.L. Taberna, P. Poizot, M. Gressier, M.J. Menu, A. Barnabe, P. Simon, J.M. Tarascon, J. Power Sources 188 (2009) 578–582.
[13] J. Hassoun, S. Panero, P. Simon, P.L. Taberna, B. Scrosati, Adv. Mater. 19 (2007) 1632–1635.
[14] H. Groult, H. El Ghallali, A. Barhoun, E. Briot, C.M. Julien, F. Lantelme, S. Borensztjan, Electrochim. Acta 56 (2011) 2656–2664.
[15] Z.P. Guo, Z.W. Zhao, H.K. Liu, S.X. Dou, Carbon 43 (2005) 1392–1399.
[16] I. Grigoriants, L. Sominski, H.L. Li, I. Ifargan, D. Aurbach, A. Gedanken, Chem. Commun. 7 (2005) 921–923.
[17] G. Derrien, J. Hassoun, S. Panero, B. Scrosati, Adv. Mater. 19 (2007) 2336–2340.
[18] W.M. Zhang, J.S. Hu, Y.G. Guo, S.F. Zheng, L.S. Zhong, W.G. Song, L.J. Wan, Adv. Mater. 20 (2008) 1160–1165.
[19] Y.C. Qiu, K.Y. Yan, S.H. Yang, Chem. Commun. 46 (2010) 8359–9361.
[20] Y. Zou, Y. Wang, ACS Nano 5 (2011) 8108–8114.
[21] Y. Yu, L. Gu, C.B. Zhu, P.A. Van Aken, J. Maier, J. Am. Chem. Soc. 131 (2009) 15984–15985.
[22] J.Z. Chen, L. Yang, S.H. Fang, S. Hirano, Electrochem. Commun. 13 (2011) 848–851.
[23] J. Hassoun, K.S. Lee, Y.K. Sun, B. Scrosati, J. Am. Chem. Soc. 133 (2011) 3139–3143.
[24] S. Jun, S.H. Joo, R. Ryoo, M. Kruk, M. Jaroniec, Z. Liu, T. Ohsuna, O. Terasaki, J. Am. Chem. Soc. 122 (2000) 10712–10713.
[25] H.S. Zhou, S.M. Zhu, M. Hbino, I. Honma, M. Ichihara, Adv. Mater. 15 (2003) 2107–2111.
[26] J. Fan, T. Wang, C.Z. Yu, B. Tu, Z.Y. Jiang, D.Y. Zhao, Adv. Mater. 16 (2004) 1432–1436.
[27 H.J. Zhang, H.H. Tao, Y. Jiang, Z. Jiao, M.H. Wu, B. Zhao, J. Power Sources 195 (2010) 2950–2955.
[28] M.Y. Cheng, B.J. Hwang, J. Power Sources 195 (2010) 4977–4983.
[29] Y.G. Wang, C.L. Zhang, S.F. Kang, B. Li, Y.Q. Wang, L.Q. Wang, X. Li, J. Mater. Chem. 21 (2011) 14420–14423.
[30] Y.G. Wang, F.Y. Zhang, Y.Q. Wang, J.W. Ren, C.L. Li, X.H. Liu, Y. Guo, Y.L. Guo, G.Z. Lu, Mater. Chem. Phys. 115 (2009) 649–655.